

Specific heat and partition function zeros for the dimer model on the checkerboard B lattice: Finite-size effects

Chi-Ning Chen,^{1,*} Chin-Kun Hu,^{1,2,†} N. Sh. Izmailian,^{3,‡} and Ming-Chya Wu^{2,4,§}

¹*Department of Physics, National Dong Hwa University, Hualien 97401, Taiwan*

²*Institute of Physics, Academia Sinica, Nankang, Taipei 11529, Taiwan*

³*Yerevan Physics Institute, Alikhanian Brothers 2, 375036 Yerevan, Armenia*

⁴*Research Center for Adaptive Data Analysis, National Central University, Zhongli, Taoyuan 32001, Taiwan*

 (Received 28 September 2018; revised manuscript received 26 November 2018; published 2 January 2019)

There are three possible classifications of the dimer weights on the bonds of the checkerboard lattice and they are denoted as checkerboard A , B , and C lattices [Phys. Rev. E **91**, 062139 (2015)]. The dimer model on the checkerboard B and C lattices has much richer critical behavior compared to the dimer model on the checkerboard A lattice. In this paper we study in full detail the dimer model on the checkerboard B lattice. The dimer model on the checkerboard B lattice has two types of critical behavior. In one limit this model is the anisotropic dimer model on rectangular lattice with algebraic decay of correlators and in another limit it is the anisotropic generalized Kasteleyn model with radically different critical behavior. We analyze the partition function of the dimer model on a $2M \times 2N$ checkerboard B lattice wrapped on a torus. We find very unusual behavior of the partition function zeros and the specific heat of the dimer model. Remarkably, the partition function zeros of finite-size systems can have very interesting structures, made of rings, concentric circles, radial line segments, or even arabesque structures. We find out that the number of the specific heat peaks and the number of circles of the partition function zeros increases with the system size. The lattice anisotropy of the model has strong effects on the behavior of the specific heat, dominating the relation between the correlation length exponent ν and the shift exponent λ , and λ is generally unequal to $1/\nu$ ($\lambda \neq 1/\nu$).

DOI: [10.1103/PhysRevE.99.012102](https://doi.org/10.1103/PhysRevE.99.012102)

I. INTRODUCTION

The classical dimer model is one of the well-known models of theoretical physics. It was first introduced in 1937 to explain the adsorption of diatomic molecules on a substrate [1]. Later, it became a general problem studied in various scientific communities with a large spectrum of applications. Dimer models have been a source of renewed interest in mathematical physics [2–10], condensed matter physics [11], computer science [12], and social science [13]. Dimer models have regained interest because of the so-called quantum dimer model, originally introduced by Rokhsar and Kivelson [14]. Besides, a recent connection between dimer models and D-brane gauge theories has been discovered [15], providing a very powerful computational tool.

From the mathematical point of view, the dimer model is extremely simple to define. We take a finite graph \mathcal{L} and consider all arrangements of dimers (dominoes), so that all sites of \mathcal{L} are covered by exactly one dimer. This is the so-called close-packed dimer model. Here we focus on the dimer model on checkerboard lattices (see Fig. 1). The checkerboard lattice is a two-dimensional (2D) system of great current interest, a setup which provides a tool to study the evolution

of physical properties as the system transits between different geometries. The checkerboard lattice is a simple rectangular lattice with anisotropic dimer weights x_1 , x_2 , y_1 , and y_2 . Each weight x_a is simply the Boltzmann factor $e^{-\epsilon_a/k_B T}$ for a dimer on a bond of type a with energy ϵ_a . In what follows, for simplicity we have chosen $k_B = 1$. There are three possible classifications of the dimer weights on the bonds of the lattice shown in Fig. 1 and they are denoted as checkerboard A , B , and C lattices, respectively [16].

It is interesting to note that the dimer model on the checkerboard lattices A , B , and C has different critical behaviors. For $x_1 = x_2$ and $y_1 = y_2$ the partition function for all three models reduces to that for the dimer model on the rectangular lattice with uniform weights. The dimer model on the rectangular lattice is critical with algebraic decay of correlators [17,18]. Such type of critical behavior can be consistently interpreted in a conformal scheme based on two conformal descriptions of the dimer model: one with $c = -2$ for the construction of a conformal field theory using a mapping of spanning trees [19–25] and the other with $c = 1$ for the height function description [26,27]. When one of the weights y_1 or y_2 is equal to zero, the dimer model on the checkerboard B lattice reduces to the dimer model on the honeycomb lattice (the Kasteleyn K_2 -model [28]), while the dimer model on the checkerboard A model reduces to the dimer model on the one-dimensional strip [10,28–30]. For the case when one of the weights x_1 , x_2 , y_1 , or y_2 is equal to zero, the dimer model on the checkerboard C model also reduces to the dimer model on the honeycomb lattice introduced by Kasteleyn

*cnchen@gms.ndhu.edu.tw

†huck@phys.sinica.edu.tw

‡izmail@yerphi.am

§mcwu@ncu.edu.tw

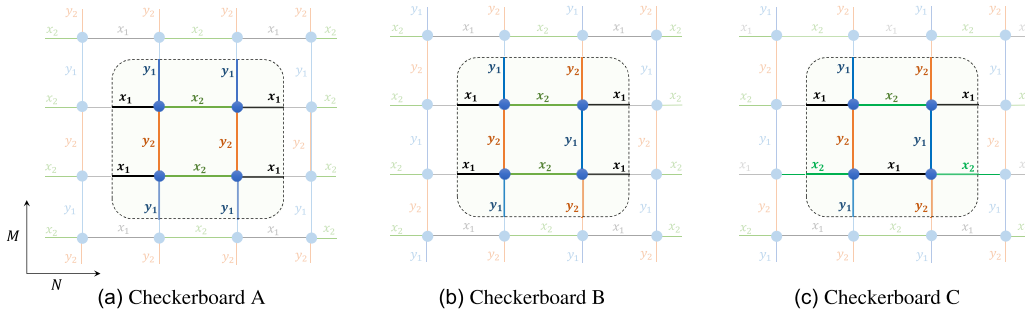


FIG. 1. The unit cells for the dimer models on the $2M \times 2N$ checkerboard lattices, $M = N = 1$.

(the Kasteleyn K_1 -model) [31], and again the dimer model on the checkerboard A model reduces to the dimer model on the one-dimensional strip. For the dimer model on the anisotropic honeycomb lattice, which is equivalent to the five-vertex model on a square lattice [32], the free energy exhibits a potassium dihydrogen phosphate-type singularity [33,34], which can be explained in the framework of the $c = 1$ conformal field theory. Thus we can see that dimer model on the checkerboard B and C lattices has much richer critical behaviors in comparison with the dimer model on the checkerboard A lattice.

The dimer model on the checkerboard A lattice was first introduced by Kasteleyn [31], who showed that the model exhibits a phase transition. Since Kasteleyn did not write an explicit form of the partition function on a finite $2M \times 2N$ checkerboard A lattice with periodic boundary conditions, it has been done in Ref. [16]. The finite-size effects of the dimer model on the checkerboard A lattice have been studied in full detail in Ref. [35]. The exact expressions of the partition function of the dimer model on the finite $2M \times 2N$ checkerboard B and C lattices with periodic boundary conditions have been obtained in Ref. [16]. The exact solution for the dimer model on the checkerboard C lattice recovers that of Cohn, Kenyon, and Propp [36] in the case $M = N$.

Finite-size scaling and corrections for critical systems, initiated more than four decades ago by Fisher and Barber [37] have attracted much attention in recent decades (see Ref. [38,39] for reviews). Finite-size effects become of practical interest due to the recent progress in fine processing technologies, which have enabled the fabrication of nanoscale materials with novel shapes [40–42]. The detailed study of the finite-size effects for free energy of the dimer model began with the work of Ferdinand [43] few years after the exact solution, and has continued in a long series of articles using analytical [19–26,30,44–51] and numerical methods [52–58] for various geometries and boundary conditions. In the present paper, we are going to study the finite-size effects of the dimer model on the finite $2M \times 2N$ checkerboard B lattice with periodic boundary conditions. We will study the finite-size effects for the specific heat $C_{2M,2N}(t)$ with the temperature-like variable t , such as the dimer weights x_a 's or their combinations. In finite-size systems, the specific heat shows a sharp peak, but it does not diverge. Finite-size properties of the specific heat $C_L(t)$ with a characteristic size of the system $L = \sqrt{4MN}$ are characterized by (i) the location of its peak, t_{pseudo} , (ii) its height $C_L(t_{\text{pseudo}})$, and its value at the infinite-volume critical point $C_\infty(t_c)$. As the system size increases, the

height of the specific heat $C_L(t_{\text{pseudo}})$ grows as

$$C(t_{\text{pseudo}}) \sim L^{\frac{2}{\nu}-d}, \quad (1)$$

according to the finite-size theory [59,60], where ν is the correlation length critical exponent and d is the dimension of the system. The peak position t_{pseudo} , is a pseudocritical point which typically approaches t_c as the characteristic size of the system L tends to infinity as

$$|t_{\text{pseudo}} - t_c| \sim L^{-\lambda}, \quad (2)$$

where λ is the shift exponent. In a classic paper, Ferdinand and Fisher [61] determined the behavior of the specific heat pseudocritical point of the Ising model on a finite plane square lattice. They found that the shift exponent for the specific heat is $\lambda = 1 = 1/\nu$. The equality of λ and $1/\nu$ is accidental and it is not a consequence of the finite-size scaling (FSS) [60]. Instead, the shift exponent is a free parameter [35,49,61–64] and the property of λ is not yet understood. The actual value of the shift exponent depends on the lattice topology [61–64] and on the parity of the lattice sites [35,49]. For lattices with a spherical topology, the two exponents were found to be $\nu = 1.00 \pm 0.06$ and $\lambda = 1.745 \pm 0.015$, significantly away from $\lambda = 1 = 1/\nu$ [62]. Janke and Kenna [64] reported the shift exponent $\lambda = 2 = 2\nu$ for the square-lattice Ising model with Brascamp-Kunz boundary conditions, again completely different from $\lambda = 1 = 1/\nu$. Very recently, Kim [63] evaluated exactly the density of states of the Ising model on a $L \times L$ square lattice with self-dual boundary conditions up to $L = 32$ and obtained $\lambda = 2$ and $\nu = 1$, clearly indicating $\lambda \neq 1/\nu$. Izmailian and Kenna [49] have found that the shift exponent can also depend on the parity of the number of lattice sites N along a given lattice axis. They found for the dimer model on the triangular lattice that the shift exponent for the specific heat is equal to 1 ($\lambda = 1$) for odd N , while for even N the shift exponent is equal to infinity ($\lambda = \infty$). In the former case, therefore, the finite-size specific-heat pseudocritical point is size dependent, while in the latter case it coincides with the critical point of the thermodynamic limit. Quite recently Izmailian, Wu and Hu [35] found for the dimer model on the finite $2M \times 2N$ checkerboard A lattice that the specific heat shift exponent is equal to infinity ($\lambda = \infty$).

For anisotropic systems like the dimer model on the checkerboard B lattice considered in this paper, the correlation length critical exponent ν and the shift exponent λ are not necessarily isotropic, and an intuitive conjecture is their values vary with the lattice shape factor and hence Eqs. (1) and (2)

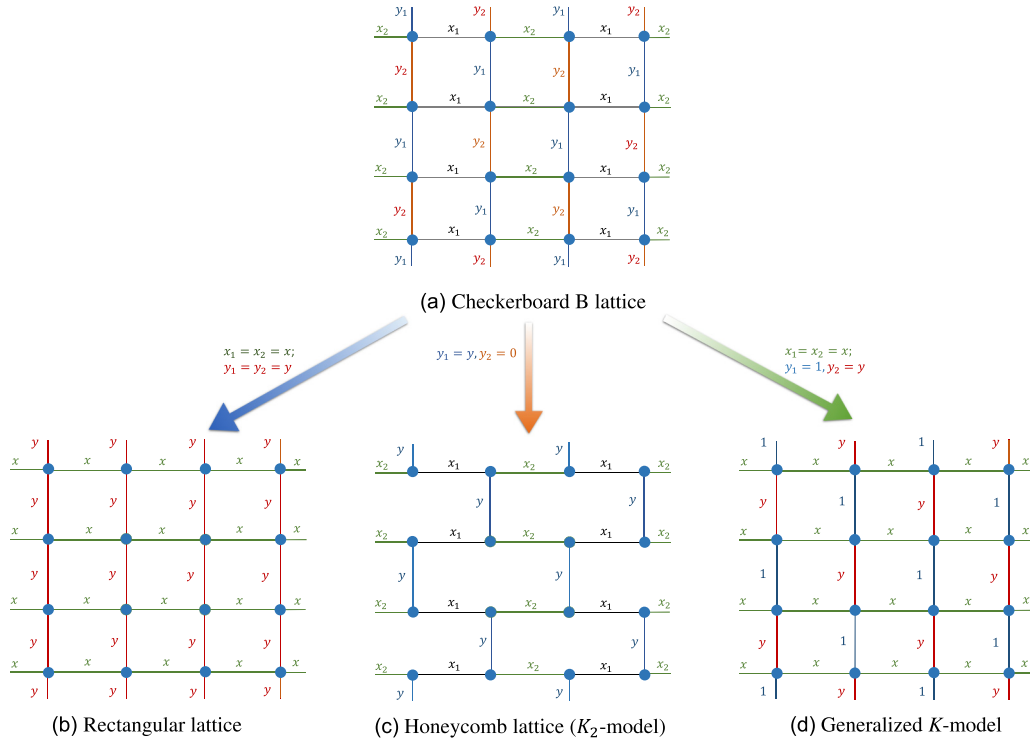


FIG. 2. The relations between (a) the checkerboard B lattice and (b) the rectangular lattice, (c) the honeycomb lattice (K_2 -model), and (d) the generalized K -model.

require a revision. One can assume that ν consists of two distinct components ν_x and ν_y respectively associated with the characteristic lengths $2N$ and $2M$, and λ consists of two independent components λ_x and λ_y . While the explicit function forms of ν as a function of ν_x and ν_y , and λ as a function of λ_x and λ_y are yet unknown, they are nontrivial and not found in this study. We will approach the issue by calculating numerically ν and λ according to Eqs. (1) and (2) at different critical points instead to check their coincidence.

The finite-size behavior of the specific heat is related to the properties of the complex temperature (Fisher) zeros of the partition function. Considerable information about the thermodynamical behavior of the system is encoded in the zeros of the partition function. For a system of finite size, the partition function Z can be written as

$$Z \propto \prod_i (z - z_i), \quad (3)$$

where z is an appropriate function of temperature and z_i 's are zeros. The specific heat of the system is a sum of the contributions from the specific heat components corresponding to the zeros. Hence, partition function zeros have attracted much attention in recent decades (see Refs. [63–68] and references therein). It has been observed that the specific heat usually exhibits various anomalies such as the two-peak Schottky-type anomaly in the low-temperature regime of the specific heat capacity [69–72], and the multipeak structure of the specific heat capacity in the frustrated magnetic system [73,74]. In this paper we will show that for finite systems the number of the specific heat peaks and the number of circles of the partition function zeros increases with the system size.

Our objective in this paper is to study the finite-size properties of the dimer model on the plane checkerboard B lattice using the techniques developed in Refs. [44] and [50] and numerical calculations. In particular we are going to obtain the patterns of the partition function zeros and the finite-size behavior of the specific heat in the vicinity of the critical point.

II. DIMER MODEL ON CHECKERBOARD B LATTICE

Let us consider the dimer model on a $2M \times 2N$ checkerboard B lattice, as shown in Fig. 2(a), under periodic boundary conditions. The partition function can be written as

$$Z_{2M,2N} = \sum x_1^{N_{x_1}} x_2^{N_{x_2}} y_1^{N_{y_1}} y_2^{N_{y_2}}, \quad (4)$$

where N_a is the number of dimers of type a and the summation is over all possible dimer configurations on the lattice. An explicit expression for the partition function of the dimer model on the $2M \times 2N$ checkerboard B lattice under periodic boundary conditions is given by [16]

$$Z_{2M,2N} = \frac{(x_1 x_2)^{MN}}{2} (-Z_{0,0}^2 + Z_{1/2,0}^2 + Z_{0,1/2}^2 + Z_{1/2,1/2}^2), \quad (5)$$

where $Z_{\alpha,\beta}^2$ is given by

$$Z_{\alpha,\beta}^2 = (x_1 x_2)^{-MN} \prod_{n=0}^{N-1} \prod_{m=0}^{M-1} \left[|x_1 e^{i\frac{\phi_{\alpha,n}}{2}} - x_2 e^{-i\frac{\phi_{\alpha,n}}{2}}|^2 - (y_1 e^{i\frac{\phi_{\beta,m}}{2}} - y_2 e^{-i\frac{\phi_{\beta,m}}{2}})^2 \right], \quad (6)$$

where $\phi_{\alpha,n} = 2\pi(n + \alpha)/N$ and $\phi_{\beta,m} = 2\pi(m + \beta)/M$.

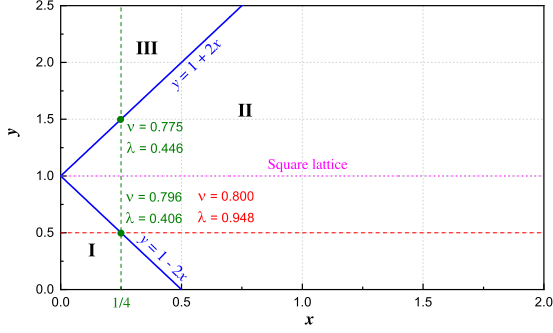


FIG. 3. The phase diagram of the generalized K -model. Phase I and II are separated by the critical line $y = 1 - 2x$, and phase II and III are separated by the critical line $y = 1 + 2x$. The red dotted line of $y = 1$ represents the dimer model on a square lattice. The correlation length critical exponent ν and the shift exponent λ are calculated in the vicinities of the critical points.

The dimer model on the checkerboard B lattice includes three different types of lattices (see Fig. 2):

(A) Dimer model on the rectangular lattice: the case $x_1 = x_2 = x$, $y_1 = y_2 = y$. The dimer model on the checkerboard B lattice in the case $x_1 = x_2 = x$ and $y_1 = y_2 = y$ reduces to the dimer model on the rectangular lattice [see Fig. 2(b)]. The dimer model on the rectangular lattice is critical and the critical behavior can be consistently interpreted in a conformal scheme based on two conformal descriptions of the dimer model: one with $c = -2$ [19–25] and the other with $c = 1$ [26,27].

(B) The generalized K -model [29,30]: the case $x_1 = x_2 = x$, $y_1 = y$, $y_2 = 1$. The dimer model on the checkerboard B lattice in the case $x_1 = x_2 = x$ and $y_1 = y$, $y_2 = 1$ reduces to the generalized K -model [see Fig. 2(d)]. The phase diagram shown in Fig. 3 for that model is very well known [29,30]. The region I is separated from the region II by the critical line $y = 1 - 2x$, and the region III is separated from the region II by the critical line $y = 1 + 2x$. In region I, the system is frozen in the ground state where the dimers are on the edges of activity 1 ($y \leq 1$). Region III is also a frozen ground state where the dimers are on the edges of activity y ($y \geq 1$). Region II is the disorder phase. The dashed line corresponds to the rectangular lattice model. Thus, we have two critical lines given by

$$\begin{aligned} (1) \quad & y = 1 + 2x, \\ (2) \quad & y = 1 - 2x. \end{aligned}$$

(C) Dimer model on the honeycomb lattice (the Kasteleyn K_2 -model [28]): the case $y_1 = y$, $y_2 = 0$. The dimer model on the checkerboard B lattice, in the case when one of the weights y_1 or y_2 , say y_2 is equal to zero and the other is a free parameter, say $y_1 = y$, reduces to the dimer model on the honeycomb lattice [see Figs. 2(c) and 3(b)].

In 1963, Kasteleyn [31] introduced the dimer model on an anisotropic honeycomb lattice, with activities x_1 , x_2 , and x_3 along the directions of three principle axes, respectively. Later that model has been called the Kasteleyn model or the K -model [75]. In 1986 Yokoi, Nagle, and Salinas [28] considered a particular variant of the K -model, which they called the K_2 -model [see Fig. 4(b)], while the original model

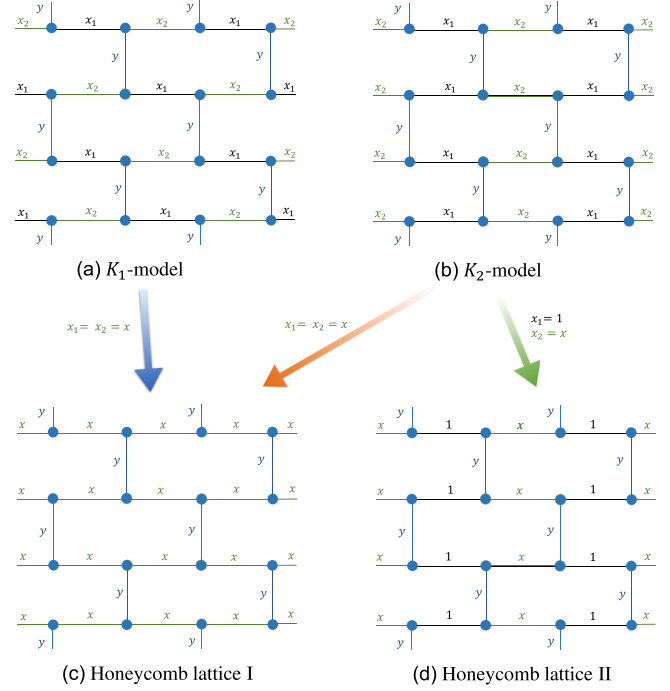


FIG. 4. The relation between (a) the K_1 -model, (b) the K_2 -model, and (c) the honeycomb lattice I and (d) the honeycomb lattice II.

studied by Kasteleyn, they called the K_1 -model [see Fig. 4(a)]. The main difference of these two models is that in the K_2 -model the arrangement of activities of the dimers obeys a rectangular symmetry rather than a hexagonal symmetry, as in the K_1 -model. The dimer model on the checkerboard C lattice, in the case when one of the weights x_1 , x_2 , y_1 , or y_2 is equal to zero, reduces to the original model studied by Kasteleyn (the K_1 -model). The K_1 -model is equivalent to the five-vertex model on a square lattice [32] and the critical behavior can be fully explained in the framework of $c = 1$ conformal field theory. The known behavior of the phase transition is that the specific heat has a square-root divergence at critical point ($T = T_c$) as T approaches T_c from above ($T \geq T_c$), while the specific heat is identically zero for all T smaller than T_c . The K_2 -model can be mapped [28] to a particular domain wall model of commensurate-incommensurate (CI) transitions introduced by Villain [76].

The dimer model on all these lattices show different types of critical behaviors, and we will consider all three cases A, B, and C. For clarity, we remark that in addition to the definition of the regular specific heat as a function of temperature T ,

$$C(T) = \frac{1}{S} \frac{1}{T^2} \frac{\partial^2}{\partial (1/T)^2} \ln Z_{2M,2N}, \quad (7)$$

where $S = 4MN$ is the area of the lattice, in this paper we will use its equivalent form, expressed by the temperaturelike variable t ,

$$C_{2M,2N}(t) = \frac{(\ln t)^2}{S} \left(t \frac{\partial}{\partial t} \right)^2 \ln Z_{2M,2N}. \quad (8)$$

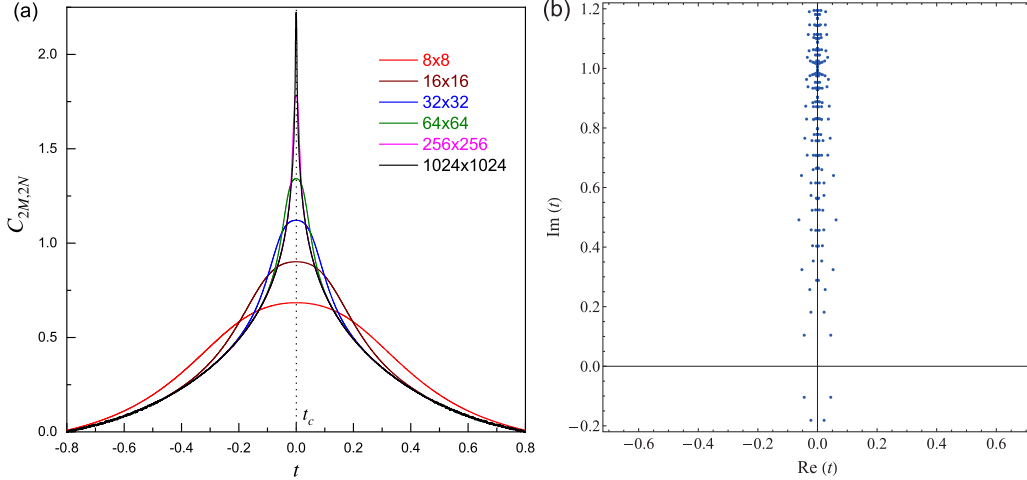


FIG. 5. The specific heat $C_{2M,2N}(t)$ of the dimer model on the $2M \times 2N$ rectangular lattice in Fig. 2(b) for $u = 1$ and $M = N$, as a function of t . Here $t^2 = (x_1 - x_2)^2/(4x_1x_2)$ and $u^2 = y^2/(4x_1x_2)$, and $t_c = 0$. (b) The partition function zeros for the lattice of $2M = 2N = 32$.

Exceptionally for the dimer model on the rectangular lattice, we will use

$$C_{2M,2N}(t) = \frac{1}{S} \frac{\partial^2}{\partial t^2} \ln Z_{2M,2N}, \quad (9)$$

instead, to conveniently demonstrate the behavior of the specific heat curve.

III. DIMER MODEL ON THE RECTANGULAR LATTICE: THE CASE $x_1 = x_2 = x$, $y_1 = y_2 = y$

One type of the critical behaviors occurs when the dimer model on the checkerboard B lattice is reduced to the dimer model on the rectangular lattice. Let us consider the critical case where the partition function of the dimer model on the checkerboard B lattice reduces to that of the dimer model on the rectangular lattice. To do so, let us first take $y_1 = y_2 = y$ in Eq. (6). Then for $Z_{\alpha,\beta}^2$ in Eq. (6) we obtain the following expression:

$$Z_{\alpha,\beta}^2 = \prod_{n=0}^{N-1} \prod_{m=0}^{M-1} 4 \left(t^2 + \sin^2 \frac{\phi_{\alpha,n}}{2} + u^2 \sin^2 \frac{\phi_{\beta,m}}{2} \right). \quad (10)$$

Here for simplicity, we have introduced two variables $t^2 = (x_1 - x_2)^2/(4x_1x_2)$ and $u^2 = y^2/(4x_1x_2)$. The critical point corresponds to $t = t_c = 0$ with an arbitrary value of u . The analysis of the dimer model on the checkerboard B lattice close to that critical point is quite similar to the analysis of the dimer model on the checkerboard A lattice [35]. Here we will consider the behavior of the specific heat and the partition function zeros near the critical point. To allow negative values of t , the specific heat $C_{2M,2N}(t)$ for this case is defined as the second derivative of the free energy with respect to t , following Eq. (9). The pseudocritical point t_{pseudo} is the value of t at which the specific heat has its maximum for a finite $2M \times 2N$ lattice. One can determine this quantity as the point where the derivative of $C_{2M,2N}(t)$ with respect to t vanishes. We take $x_1 = x_2 = x$ to demonstrate the x -dependence of the critical behavior. In Figs. 5(a) and 6(a), we plot, respectively, the t - and x -dependence of the specific heat for the case of

$u = 1$ with different lattice sizes up to 1024×1024 . We can see from Fig. 5(a) that the position of the specific-heat peak t_{pseudo} is equal exactly to zero. Therefore, the maximum of the specific heat (at t_{pseudo}) always occurs at vanishing reduced temperature for any finite $2M \times 2N$ lattice and coincides with the critical point t_c in the thermodynamic limit ($t_{\text{pseudo}} = t_c = 0$). Hence, from Eq. (2) we find that the shift exponent is infinity ($\lambda = \infty$), apparently different from the inverse of the correlation length critical exponent ($\lambda \neq 1/\nu$).

Figures 5(b) and 6(b), respectively, show the distribution of the partition function zeros in the complex t and complex x planes for the lattice size $2M \times 2N = 32 \times 32$ in Figs. 5(a) and 6(a). The distribution of the zeros near $\text{Re}(t) = 0$ in Fig. 5(b) manifests the sharp peak of the specific heat curve at the critical point $t_c = 0$ in Fig. 5(a) even for small system sizes. Similarly, the distribution of the partition function zeros in a ring of radius 1 that intersects with the real axis at $\text{Re}(x) = 1$ in Fig. 6(b) features the dominant contributions of the zeros to the specific heat in the vicinity of the critical point $x_c = 1$ in Fig. 6(a) regardless of the system size.

IV. THE GENERALIZED K -MODEL: THE CASE

$$x_1 = x_2 = x, \quad y_1 = y, \quad y_2 = 1$$

Another type of the critical behaviors occurs when the dimer model on the checkerboard B lattice is reduced to the generalized K -model in the case $x_1 = x_2 = x$, $y_1 = y$, $y_2 = 1$. The partition function of the generalized K -model is given by Eq. (5), whereas $Z_{\alpha,\beta}^2$ reads as

$$Z_{\alpha,\beta}^2 = x^{-2MN} \prod_{n=0}^{N-1} \prod_{m=0}^{M-1} \left[4x^2 \sin^2 \left(\frac{\phi_{\alpha,n}}{2} \right) - \left(ye^{i\frac{\phi_{\beta,m}}{2}} - e^{-i\frac{\phi_{\beta,m}}{2}} \right)^2 \right]. \quad (11)$$

The phase diagram for this model shown in Fig. 3 is very well known [29,30]. To see the critical behaviors of this model, we consider a particular situation with $x = 1/4$ and another situation with $y = 1/2$, which, respectively, correspond to

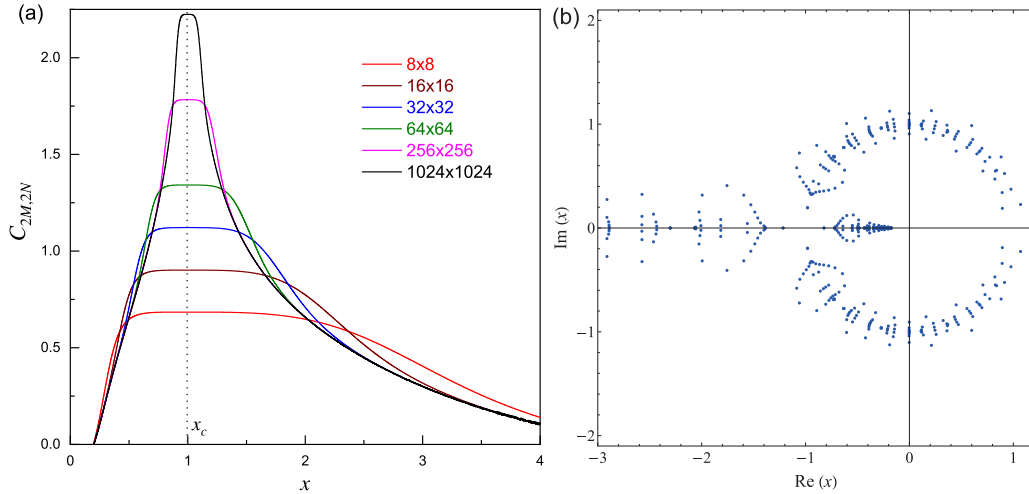


FIG. 6. The specific heat $C_{2M,2N}(x)$ of the dimer model on the $2M \times 2N$ rectangular lattice in Fig. 2(b) for $u = 1$ and $M = N$, as a function of x . Here $u^2 = y^2/(4x^2)$ and $x_c = 1$. (b) The partition function zeros for the lattice of $2M = 2N = 32$.

varying y along the green dashed line of $x = 1/4$ and varying x along the red dashed line of $y = 1/2$ in Fig. 3.

The specific heat and the partition function zeros for the case $x = 1/4$ are shown in the Fig. 7. There are two peaks at $y = 1/2$ and $y = 3/2$ in the specific heat curves of Fig. 7(a), corresponding to the intersections of the line $x = 1/4$ with the critical line $y_{c1} = 1 - 2x$ at $y_{c2} = 1/2$ and with the critical line $y = 1 + 2x$ at $y = 3/2$ in the phase diagram of Fig. 3. These two peaks have unequal heights as they are phase transitions through different phase boundaries. This scenario is also depicted by the distribution pattern of the partition function zeros in Fig. 7(b) for the lattice of $2M = 2N = 48$. The two ends of the radial line distribution of zeros at the real axis [i.e., $\text{Re}(y)$] in Fig. 7(b) correspond to the critical points y_{c1} and y_{c2} in Fig. 7(a).

We determine the correlation length critical exponent ν and the shift exponent λ using Eqs. (1) and (2) and $d = 2$. We numerically calculate the specific heat $C_{2M,2M}(y)$ as a function of y for various lattice sizes, collect the data of the specific heat peak $C_{2M,2M}(y_{\text{pseudo}})$ and the pseudocritical point

y_{pseudo} to plot $\ln C_{2M,2M}(y_{\text{pseudo}})$ versus $\ln(2M)$ and $|y_c - y_{\text{pseudo}}|$ versus $\ln(2M)$, then use the linear fitting function in Originlab Origin Pro to fit the data and estimate errors. Note that $y_c - y_{\text{pseudo}}$ changes sign as the system size increases, and hence $|y_c - y_{\text{pseudo}}|$ versus $\ln(2M)$ is not linear. We fit the linear regime closest to $|y_c - y_{\text{pseudo}}| = 0$ to determine λ . Our results are $\nu = 0.796 \pm 0.037$ and $\lambda = 0.406 \pm 0.038$ for $y_{c1} = 1/2$, and $\nu = 0.775 \pm 0.041$ and $\lambda = 0.446 \pm 0.119$ for $y_{c2} = 3/2$.

Furthermore, the specific heat and the partition function zeros for the case $y = 1/2$ are shown in Fig. 8. The single peak at $x = 1/4$ in Fig. 8(a) represents the critical behavior at the intersection of the line $y = 1/2$ with the critical line $y = 1 + 2x$ at $x = 1/4$. The dilute, radial, and ring distribution pattern of the partition function zeros in Fig. 8(b) for the lattice of $2M = 2N = 48$ is quite different from that of Fig. 7(b). The location of the critical point is determined by the intersection of the smallest ring with the real axis at $\text{Re}(x) = 1/4$, corresponding to the peak in Fig. 8(a). For this case, we have $\nu = 0.800 \pm 0.001$ and $\lambda = 0.948 \pm 0.004$. Remarkably, the shift

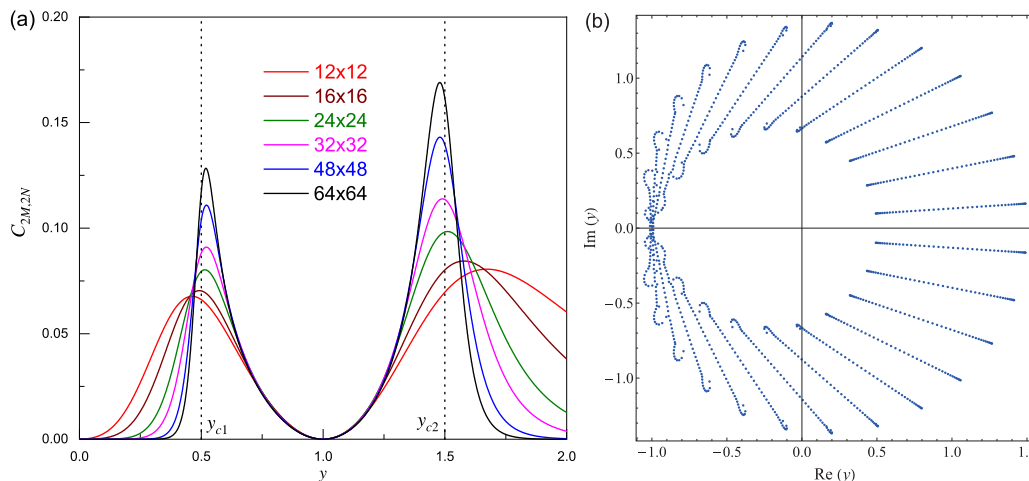


FIG. 7. (a) The specific heat $C_{2M,2N}(x)$ as a function of x for the generalized K -model in Fig. 2(d) with $x = 1/4$. Here $y_{c1} = 1/2$ and $y_{c2} = 3/2$. (b) The partition function zeros for the lattice of $2M = 2N = 48$.

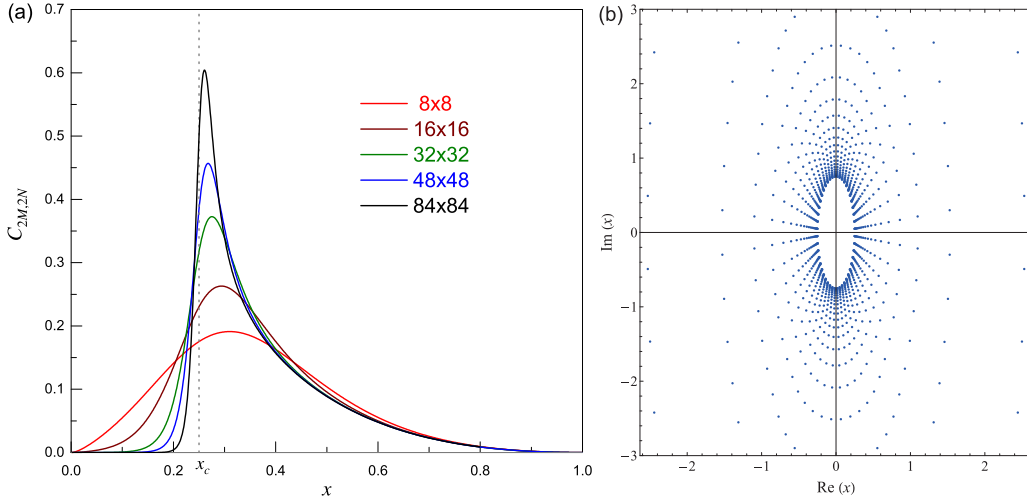


FIG. 8. (a) The specific heat $C_{2M,2N}(x)$ as a function of x for the generalized K -model in Fig. 2(d) with $y = 1/2$. Here $x_c = 1/4$. (b) The partition function zeros for the lattice of $2M = 2N = 48$.

exponent λ is anisotropic at $x_c = 1/4$, $y_c = 1/2$, as shown in Fig. 6. Again, the analysis of the correlation length critical exponent ν and the shift exponent λ in this case suggests they are not coincident ($\lambda \neq 1/\nu$).

V. DIMER MODEL ON THE HONEYCOMB LATTICE (K_2 -MODEL): THE CASE $y_2 = 0$

Next, we consider in full detail the case $y_2 = 0$, when the dimer model on the checkerboard B lattice turns to the honeycomb lattice model or the K_2 -model [28,29]. Here, we will consider two cases: the first case when the dimer activities x_1 and x_2 are equal [Fig. 4(c)] is called the honeycomb lattice I, and the second case when they are not [Fig. 4(d)] is referred to the honeycomb lattice II. For the first case, we have set $x_1 = x_2 = x$ [see Fig. 4(c)] and for the second case without losing generality we choose $x_1 = 1$ and $x_2 = x$ [see Fig. 4(d)].

A. The case $x_1 = x_2 = x$

For the first case ($x_1 = x_2 = x$) the partition function of the model is given by Eq. (5), where $Z_{\alpha,\beta}^2$ can be written as

$$\begin{aligned} Z_{\alpha,\beta}^2 &= x^{-2MN} \prod_{n=0}^{N-1} \prod_{m=0}^{M-1} \left(x^2 \left| e^{i\frac{\phi_{\alpha,n}}{2}} - e^{-i\frac{\phi_{\alpha,n}}{2}} \right|^2 - y^2 e^{i\phi_{\beta,m}} \right) \\ &= \prod_{n=0}^{N-1} \prod_{m=0}^{M-1} 4 \left(\sin^2 \frac{\phi_{\alpha,n}}{2} - \frac{y^2}{4x^2} e^{i\phi_{\beta,m}} \right). \end{aligned} \quad (12)$$

It is easy to see from Eq. (12) that $Z_{\alpha,\beta}^2$ is a function of the new variable u :

$$u = \frac{y}{2x}. \quad (13)$$

With the help of the identity

$$\prod_{m=0}^{M-1} [a - b e^{i\frac{2\pi(m+\beta)}{M}}] = a^M - b^M e^{i2\pi\beta}, \quad (14)$$

the $Z_{\alpha,\beta}^2$ can be transformed into a simpler form

$$\begin{aligned} Z_{\alpha,\beta}^2 &= \prod_{n=0}^{N-1} 4^M \left[\sin^{2M} \frac{\pi(n+\alpha)}{N} - e^{i2\pi\beta} u^{2M} \right] \\ &= (2u)^{2MN} \prod_{n=0}^{N-1} [e^{2M\omega_1(\frac{\pi(n+\alpha)}{N})} \pm 1], \end{aligned} \quad (15)$$

where $+$ and $-$ signs stand for $\beta = 1/2$ and 0 , respectively. Here we have introduced $\omega_1(k)$ defined as

$$\omega_1(k) = \ln \left(\frac{1}{u} \sin k \right). \quad (16)$$

Now the $\ln Z_{\alpha,\beta}$ can be written as

$$\begin{aligned} \ln Z_{\alpha,\beta} &= MN \ln(2u) \\ &+ \frac{1}{2} \operatorname{Re} \sum_{n=0}^{N-1} \ln [e^{2M\omega_1(\frac{\pi(n+\alpha)}{N})} \pm 1]. \end{aligned} \quad (17)$$

The phase diagram of this case is shown in Fig. 9. The system undergoes a phase transition at the critical line $y = 2x$ or at the critical point $u = u_c = 1$.

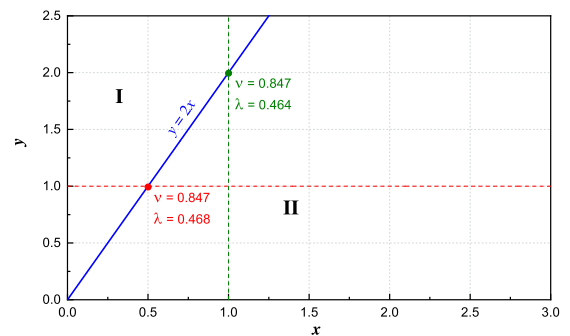


FIG. 9. The phase diagram of the K_2 -model honeycomb lattice I of Fig. 4(c). The correlation length critical exponent ν and the shift exponent λ are calculated in the vicinities of the critical points.

One can define the density of horizontal dimers $\rho_{2M,2N}(x)$ and the density of vertical dimers $\rho_{2M,2N}(y)$ as

$$\rho_{2M,2N}(x) = \frac{x}{S} \frac{\partial}{\partial x} \ln Z_{2M,2N}, \quad (18)$$

$$\rho_{2M,2N}(y) = \frac{y}{S} \frac{\partial}{\partial y} \ln Z_{2M,2N}, \quad (19)$$

and the definition of the specific heat follows Eq. (7). Let us denote by $Z(u)$,

$$Z(u) = -Z_{0,0}^2 + Z_{1/2,0}^2 + Z_{0,1/2}^2 + Z_{1/2,1/2}^2, \quad (20)$$

then the partition function of the model can be written as

$$Z_{2M,2N} = \frac{x^{S/2}}{2} Z(u). \quad (21)$$

Now one can easily show that the density of horizontal dimers $\rho_{2M,2N}(x)$, the density of vertical dimers $\rho_{2M,2N}(y)$, and the specific heat $C(T)$ can be rewritten in the following form:

$$\rho_{2M,2N}(x) = \frac{1}{2} - \frac{u}{S} \frac{\partial}{\partial u} \ln Z(u), \quad (22)$$

$$\rho_{2M,2N}(y) = \frac{u}{S} \frac{\partial}{\partial u} \ln Z(u), \quad (23)$$

and

$$C(T) = (\ln 2u)^2 \left[\frac{u}{S} \frac{\partial}{\partial u} \ln Z(u) + \frac{u^2}{S} \frac{\partial^2}{\partial u^2} \ln Z(u) \right]. \quad (24)$$

We found that in the thermodynamic limit ($M, N \rightarrow \infty$), the density of horizontal dimers $\rho_{2M,2N}(x)$, the density of vertical dimers $\rho_{2M,2N}(y)$, and the specific heat $C(T)$ for $u > u_c$ ($u_c = 1$) are given by

$$\rho_x = \lim_{M,N \rightarrow \infty} \rho_{2M,2N}(x) = 0, \quad (25)$$

$$\rho_y = \lim_{M,N \rightarrow \infty} \rho_{2M,2N}(y) = \frac{1}{2}, \quad (26)$$

$$C_\infty = 0, \quad (27)$$

while for $u < u_c$ ($u_c = 1$) we obtain

$$\lim_{M,N \rightarrow \infty} \frac{u}{S} \frac{\partial}{\partial u} \ln Z = \frac{1}{2} - \frac{\cos^{-1} u}{\pi}, \quad (28)$$

$$\lim_{M,N \rightarrow \infty} \frac{u^2}{S} \frac{\partial^2}{\partial u^2} \ln Z = -\frac{1}{2} + \frac{\cos^{-1} u}{\pi} + \frac{u}{\pi \sqrt{1-u^2}}, \quad (29)$$

and

$$\rho_x = \frac{\cos^{-1} u}{\pi}, \quad (30)$$

$$\rho_y = \frac{1}{2} - \frac{\cos^{-1} u}{\pi}, \quad (31)$$

$$C_\infty = \frac{u}{\pi} \frac{(\ln 2u)^2}{\sqrt{1-u^2}}. \quad (32)$$

Let us now, for example, consider three cases, namely, the case $y = 1$ ($\epsilon_y = 0$), the case $x = 1$ ($\epsilon_x = 0$), and the case $x = 1/2$. The first case ($y = 1$) has been considered in Ref. [75]. The critical point ($u_c = 1$) for that case corresponds

to $x_c = 1/2$. From Eqs. (25), (27), (30), and (32) we can easily reobtain the result of Ref. [75]. In particular, the density of horizontal dimers ρ_x and the specific heat $C_\infty(x)$ are given by, for $x \leq \frac{1}{2}$,

$$\rho_x = C_\infty(x) = 0, \quad (33)$$

and for $x > 1/2$,

$$\rho_x = \frac{1}{\pi} \cos^{-1} \left(\frac{1}{2x} \right), \quad (34)$$

$$C_\infty(x) = \frac{1}{\pi} \frac{(\ln x)^2}{\sqrt{4x^2 - 1}}. \quad (35)$$

The equations above show that the system undergoes a phase transition at the critical point $x = x_c = 1/2$. The specific heat $C_{2M,2N}$ of this case with $y = 1$, as a function of x is shown in Fig. 10(a) for fixed $2M = 32$, and in Fig. 11(a) for fixed $2N = 32$. There are multiple peaks in the specific heat curves which are associated with the distributions of the partition function zeros in Figs. 10(b) and 10(c), and Figs. 11(b) and 11(c). The partition function zeros plotted in the complex x plane for the lattice of $2M \times 2N = 32 \times 128$ has a structure made of concentric circles in a larger scale [see Fig. 10(b)] and radial line segments in a smaller scale [see Fig. 10(c)]. Meanwhile, the partition function zeros for the lattice of $2M \times 2N = 128 \times 32$ shows concentric circles in both large and small scales [see Figs. 11(b) and 11(c)]. The peak in the specific heat is a result of the ring distribution pattern of zeros, and the number of peaks, corresponding to the number of the concentric rings, is in principle proportional to the lattice size $2N$, or more precisely, equal to N . Meanwhile, the heights of the peaks are associated with the lattice size $2M$, due to the contribution of $2M$ zeros in a ring. It follows that the height of the peak closest to x_c in Fig. 10(a) is limited by the fixed $2M = 32$ and does not grow with the increasing $2N$, while the peaks far from x_c are smeared out when $2N$ becomes larger. On the contrary, the locations of the multiple peaks in Fig. 11(a) are roughly fixed for the fixed $2N = 32$ and the heights of peaks grow with the increasing $2M$. Hence, the lattice anisotropy has strong effects on the behaviors of the specific heat for the model on finite lattices. Interestingly, the height of the peak closest to x_c does not grow more significantly.

The above scenario can be understood by considering the arrangement of dimers on a honeycomb lattice which is equivalent to a brick lattice. On the brick lattice, there is a constraint that when a horizontal x dimer is placed, another two x dimers must be placed in the row below and the row above. This is due to the fact that the horizontal x dimer will block two neighboring vertical y dimers, and the endpoints of the two y dimers must be covered by another two x dimers. Thus, the number of x dimers of a legal dimer covering state can only be $0, 2M, 4M, \dots$. When the weight of the ground state is y^{2MN} , the weight of the first excited state is $x^{2M} y^{2M(N-1)}$, and the weight of the second excited state is $x^{2(2M)} y^{2M(N-2)}$, etc. All these terms will appear in the expansion of Eq. (3). Therefore, when x value is fixed, the expansion of $Z(y)$ is an N th degree polynomial of y^{2M} , and when y value is fixed, the expansion of $Z(x)$ is an N th degree polynomial of x^{2M} . As a result, for the case of honeycomb lattice I (and II with x fixed), the partition function zeros have a structure of N

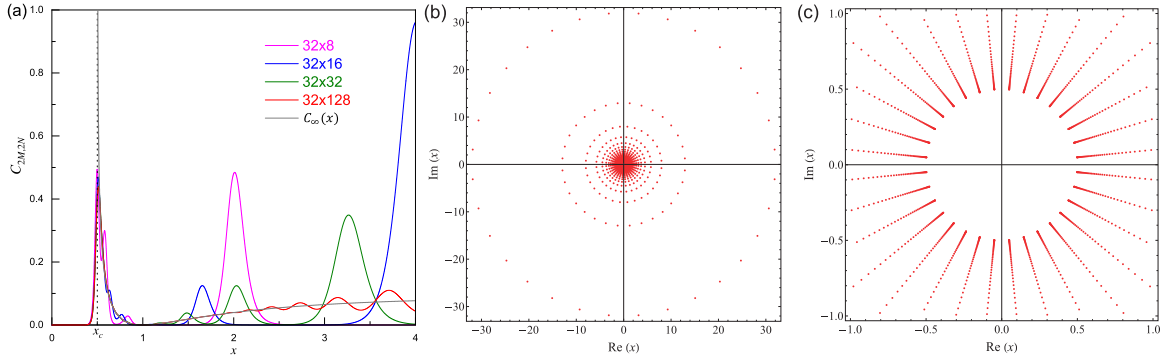


FIG. 10. (a) The specific heat $C_{2M,2N}(x)$ of the K_2 -model honeycomb lattice I in Fig. 4(c) and $y = 1$, as a function of x , for fixed $2M = 32$. Here $x_c = 1/2$ and $C_{\infty}(x)$ is defined in Eq. (35). (b) The partition function zeros for the lattice of $2M \times 2N = 32 \times 128$. (c) The zoom-in of (b).

concentric circles, each with $2M$ zeros distributed uniformly in it. While these zeros look more like concentric circles with large M and small N , they look more like radial line segments with small M and large N . The associated specific heat in the former case shows more peaks than in the latter case, and they are distinct: When M goes to infinity and N is kept finite in the former case, the first zeros of all N circles indeed touch the real axis, which leads to N phase transitions. The uniform distribution of zeros on the circles indicates the transitions are first-order. The sequence of first-order transitions of the K model has been studied for some time [30,77], while our analysis of the partition function zeros provides a clear picture for this intriguing property. When M is kept finite and N goes to infinity in the latter case, the zeros do not touch the real axis and there is no phase transition in the region of the phase diagram for the disorder phase, except in the phase boundary where the Kasteleyn transition takes place. The zeros in radial line segments close to the phase boundary are denser than the zeros away from the phase boundary. Although no zeros touch the real axis, when N increases, the accumulation of zeros near the phase boundary contributes to a larger and larger specific heat, which is the indication of the Kasteleyn transition [31]. Away from the phase boundary, the contribution from close zeros to the specific heat always cancels each other. Hence, in the thermodynamic limit when both M and N go to infinity, the specific heat of the K model shows only one peak, but not many peaks.

For the K_2 -model honeycomb lattice I, in the thermodynamic limit (i.e., infinite system size on both M and N), there is only a single peak at x_c , which is a result of gradual peak reduction from the multippeak version of finite-size cases. For finite systems, however, single-peak specific curves always take place in the vicinity of the critical point when N is much larger than M , and vice versa. The condition of $M \ll N$ can be conveniently achieved by considering particular system shapes with the shape factor ξ defined as

$$\xi = \frac{M^2}{N}, \tag{36}$$

and taking values of $\xi \lesssim 1$. The cases of the specific heat of the K_2 -model honeycomb lattice I with $y = 1$ and $\xi \lesssim 1$ having a single peak are shown in Fig. 12(a) ($\xi = 1/4$) and Fig. 13(a) ($\xi = 1$), and multiple peak cases are shown in Figs. 12(b) ($\xi = 4$) and 12(c) ($\xi = 64$). The lattice anisotropy further has effects on the correlation length critical exponent ν and the shift exponent λ . For $\xi = 1$, we have numerically calculated ν and λ according to Eqs. (1) and (2) and the result is $\nu = 8.847 \pm 0.003$ and $\lambda = 0.468 \pm 0.023$.

Figure 13(b) shows the density of horizontal dimers $\rho_{2M,2N}(x)$ as a function of x for $y = 1$. Figure 13 shows the consistency between numerical calculations and the exact expression of $C_{\infty}(x)$ in Eq. (35), and ρ_x in Eq. (34). By recalling that $x = e^{-\epsilon_x/T}$ the critical temperature is $T_c = \epsilon_x / \ln 2$. The Eq. (35) demonstrates $t_r^{-1/2}$ dependence of the bulk specific

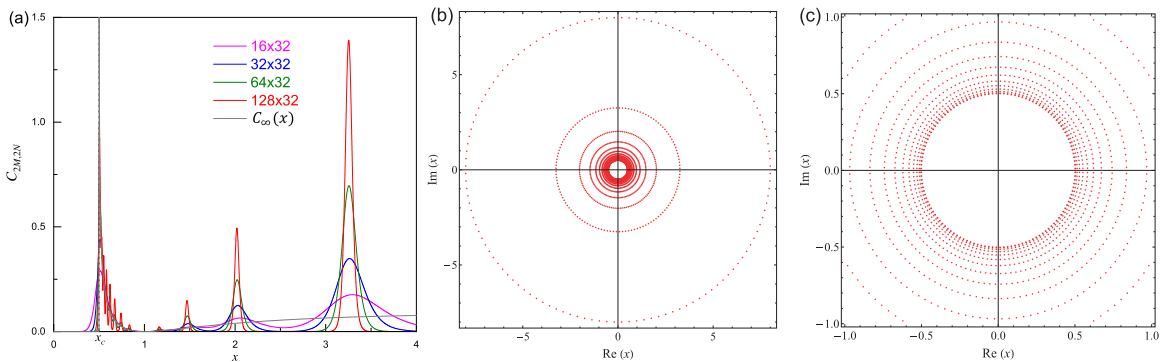


FIG. 11. (a) The specific heat $C_{2M,2N}(x)$ of the K_2 -model honeycomb lattice I in Fig. 4(c) and $y = 1$, as a function of x , for fixed $2N = 32$. Here $x_c = 1/2$ and $C_{\infty}(x)$ is defined in Eq. (35). (b) The partition function zeros for the lattice of $2M \times 2N = 128 \times 32$. (c) The zoom-in of (b).

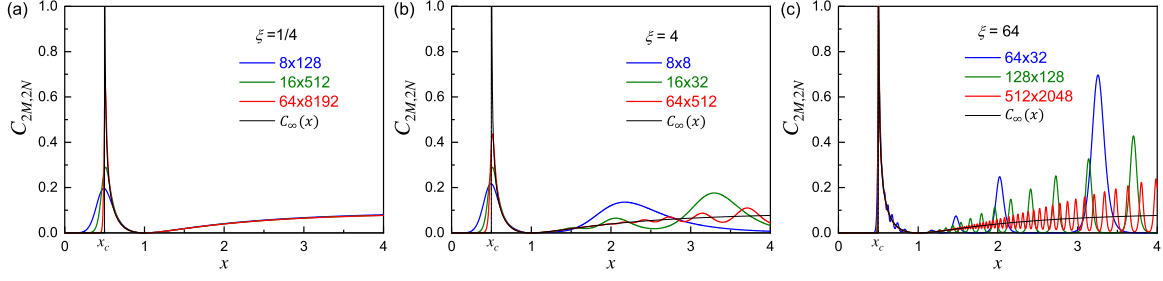


FIG. 12. The specific heat $C_{2M,2N}(x)$ of the K_2 -model honeycomb lattice I of Fig. 4(c) and $y = 1$, as a function of x for the shape factor (a) $\xi = 1/4$, (b) $\xi = 4$, and (c) $\xi = 64$. Here $x_c = 1/2$, and $C_\infty(x)$ is defined in Eq. (35).

heat as $t_r \rightarrow 0+$, where

$$t_r = \frac{T - T_c}{T_c} \quad (37)$$

is the reduced temperature.

Let us now consider the second case, namely, $x = 1$ ($\epsilon_x = 0$). The critical point ($u_c = 1$) for this case corresponds to $y_c = 2$. From Eqs. (26), (27), (31), and (32) we can obtain that the density of vertical dimers ρ_y and the specific heat $C_\infty(y)$, for $y \geq 2$,

$$\rho_y = \frac{1}{2}, \quad C_\infty(y) = -\frac{1}{2}, \quad (38)$$

and for $y < 2$,

$$\rho_y = \frac{1}{2} - \frac{1}{\pi} \cos^{-1} \left(\frac{y}{2} \right), \quad (39)$$

$$C_\infty(y) = \frac{y}{\pi} \frac{(\ln y)^2}{\sqrt{4 - y^2}}. \quad (40)$$

These equations show that the system undergoes a phase transition at the critical point $y = y_c = 2$. By recalling that $y = e^{-\epsilon_y/T}$ the critical temperature is $T_c = -\epsilon_y/\ln 2$. The Eq. (40) demonstrates $t_r^{-1/2}$ dependence of the bulk specific heat as $t_r \rightarrow 0+$. The main difference from the first case is that the energy of y dimers at the critical point is negative, while in the first case the energy of x dimers at the critical point is positive. Figures 14(a) and 14(b), respectively, show the specific heat $C_{2M,2N}$ and the density of vertical dimers $\rho_{2M,2N}$ as functions of y for $x = 1$ and $\xi = 1$. The small but sharp peaks near $y = 0$ for smaller lattices are relics of competition of the horizontal dimers with a fixed weight $x = 1$ and the vertical dimers with a varying weight y . The numerical results show consistency with Eqs. (40) and (39). The correlation length critical exponent ν and the shift exponent λ for $\xi = 1$ have been calculated numerically, and the results are $\nu = 0.847 \pm 0.003$ and $\lambda = 0.464 \pm 0.023$. This value of the shift exponent is the same as the $y = 1$ case.

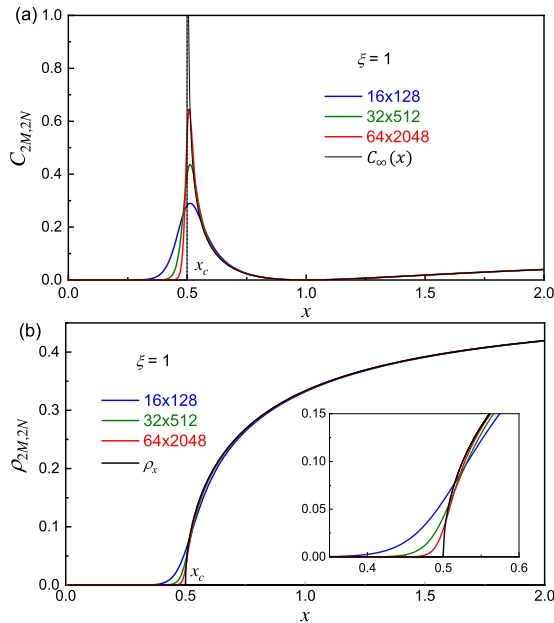


FIG. 13. The specific heat $C_{2M,2N}(x)$ of the K_2 -model honeycomb lattice I in Fig. 4(c) for $y = 1$ and $\xi = 1$, as a function of x . Here $x_c = 1/2$, and $C_\infty(x)$ is defined in Eq. (35). (b) The density of horizontal dimers $\rho_{2M,2N}$ as a function of x . ρ_x is defined in Eq. (34). The inset shows the zoom-in near $x_c = 1/2$.

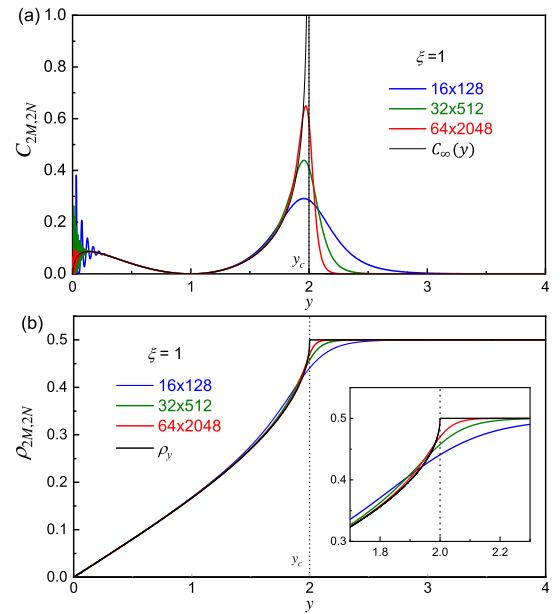


FIG. 14. The specific heat $C_{2M,2N}(y)$ of the K_2 -model honeycomb lattice I in Fig. 4(c) for $x = 1$ and $\xi = 1$, as a function of y . Here $y_c = 2$ and $C_\infty(y)$ is defined in Eq. (40). (b) The density of vertical dimers $\rho_{2M,2N}$ as a function of y . ρ_y is defined in Eq. (39). The inset shows the zoom-in near $y_c = 2$.

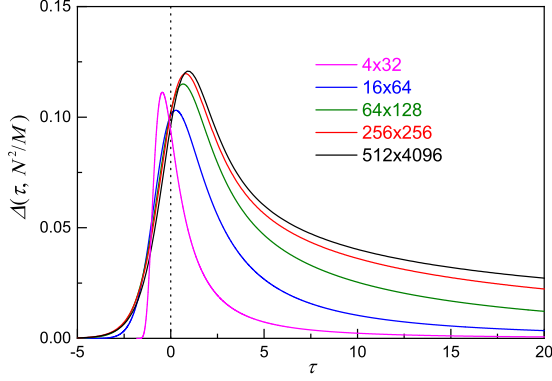


FIG. 15. The scaling function of the specific heat $\Delta(\tau, N^2/M)$ as a function of the scaled temperature τ for the K_2 -model honeycomb lattice I in Fig. 4(c) with $y = 1$ and $N^2/M = 128$.

The finite-size effect for the critical point for the first case of the model ($y = 1$) has been studied in Ref. [30]. The finite-size scaling function is a function of a scaled temperature variable τ and a factor N^2/M which is associated with the argument in the asymptotic expansion of the partition function. Here, we define the scaled temperature τ as

$$\tau = \frac{MN^2}{M + N^2} t_r. \quad (41)$$

According to Ref. [30], the specific heat $C_{2M,2N}(t_r)$ can then be written as

$$C_{2M,2N}(t_r) \approx \Delta\left(\tau, \frac{N^2}{M}\right) \mathcal{M}^{\frac{1}{2}}, \quad (42)$$

where $\Delta(\tau, N^2/M)$ is the scaling function of the specific heat and \mathcal{M} is a size-dependent variable defined as

$$\mathcal{M} = \frac{MN^2}{M + N^2}. \quad (43)$$

To demonstrate a well-behaved scaling function $\Delta(\tau, N^2/M)$, we choose the lattice with the specific heat curve having a single peak in the vicinity of the critical point. Figure 15 shows the scaling function $\Delta(\tau, N^2/M)$ as a function of the scaled temperature τ for $N^2/M = 128$. As the lattice size increases, the scaling function $\Delta(\tau, N^2/M)$ approaches to a specified function form of infinite system size. The value of the pseudocritical point t_{pseduo} varies from $t_{\text{pseduo}} < t_c$ for smaller lattice to $t_{\text{pseduo}} > 0$ for larger lattice and the scaling function of a small lattice does not have a good match with those of larger lattices. Also, unlike the finite-size scaling function [78], the scaling functions defined in Eq. (42) for different lattice sizes do not coincide at $\tau = 0$ and their peaks depart from $\tau = 0$ with the increase of system size as a result of the appearance of the scale variable \mathcal{M} in the scaled temperature τ defined in Eq. (41).

B. The case $x_1 = 1, x_2 = x$

Let us consider in full detail the second case, namely $x_1 = 1, x_2 = x$. For this case, the partition function of the model is

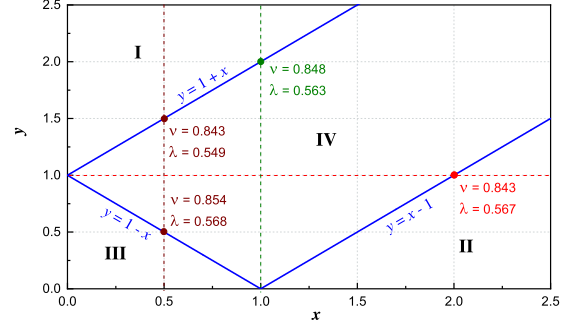


FIG. 16. The phase diagram of the dimer model on the K_2 -model honeycomb lattice II in Fig. 4(d). The correlation length critical exponent ν and the shift exponent λ are calculated in the vicinities of the critical points.

given by Eq. (5), where $Z_{\alpha,\beta}^2$ can be written as

$$\begin{aligned} Z_{\alpha,\beta}^2 &= x^{-MN} \prod_{n=0}^{N-1} \prod_{m=0}^{M-1} \left(\left| e^{i\frac{\phi_{\alpha,n}}{2}} - x e^{-i\frac{\phi_{\alpha,n}}{2}} \right|^2 - y^2 e^{i\phi_{\beta,m}} \right) \\ &= \prod_{n=0}^{N-1} \prod_{m=0}^{M-1} 4 \left[\sin^2 \frac{\phi_{\alpha,n}}{2} + \frac{(1-x)^2}{4x} - \frac{y^2}{4x} e^{i\phi_{\beta,m}} \right] \\ &= \prod_{n=0}^{N-1} 4^M \left\{ \left[\sin^2 \frac{\pi(n+\alpha)}{N} + \frac{(1-x)^2}{4x} \right]^M \right. \\ &\quad \left. - e^{2\pi i\beta} \left(\frac{y^2}{4x} \right)^M \right\} \\ &= \left(\frac{y^2}{x} \right)^{MN} \prod_{n=0}^{N-1} \left[e^{2M\omega\left(\frac{\pi(n+\alpha)}{N}\right) - 2\pi i\beta} - 1 \right], \end{aligned} \quad (44)$$

where we have introduced $\omega(k)$ defined as

$$\omega(k) = \frac{1}{2} \ln \left[\frac{4x}{y^2} \sin^2 k + \frac{(1-x)^2}{y^2} \right]. \quad (45)$$

Now the $\ln Z_{\alpha,\beta}$ can be written as

$$\begin{aligned} \ln Z_{\alpha,\beta} &= \frac{MN}{2} \ln \frac{y^2}{x} \\ &\quad + \frac{1}{2} \text{Re} \sum_{n=0}^{N-1} \ln \left[e^{2M\omega\left(\frac{\pi(n+\alpha)}{N}\right) - 2\pi i\beta} - 1 \right]. \end{aligned} \quad (46)$$

The phase diagram for that model is also very well known [29]. In the phase diagram of Fig. 16, the region I is separated from the region IV by the critical line $y = 1 + x$, the region II is separated from the region IV by the critical line $y = x - 1$, and the region III is separated from the region IV by the critical line $y = 1 - x$. Thus, we have three critical lines given by

- (1) $y = x + 1,$
- (2) $y = x - 1,$
- (3) $y = 1 - x.$

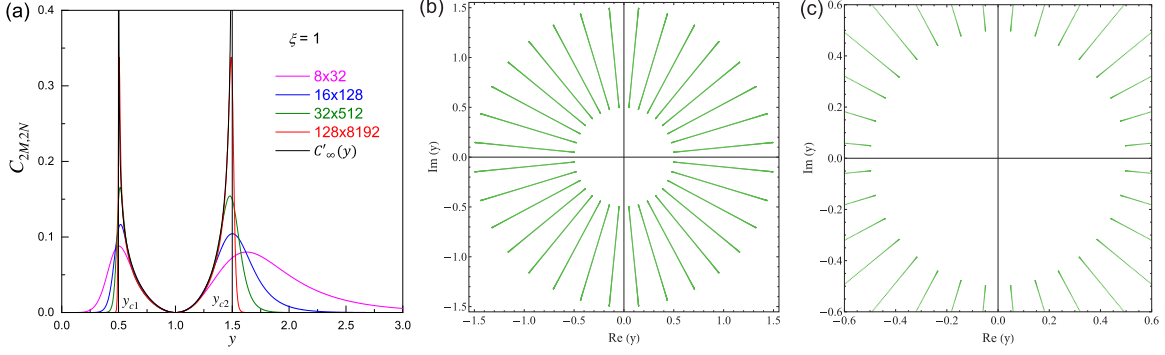


FIG. 17. The specific heat $C_{2M,2N}(y)$ of the K_2 -model honeycomb lattice II in Fig. 4(d) and $x = 1/2$ with the shape factor $\xi = 1$, as a function of y . Here $y_{c1} = 1/2$ and $y_{c2} = 3/2$, and $C'_{\infty}(y)$ is defined in Eq. (47). (b) The partition function zeros for the lattice of $2M \times 2N = 32 \times 512$. (c) The zoom-in of (b).

In regions I, II, and III, the system is frozen in the ground state, where the dimers are on the edges of activity 1, x , and y , respectively. Region IV is the disorder phase.

We analyze the thermodynamic properties of the system by calculating the specific heat and the partition function zeros of the lattice. Using Eqs. (5) and (44), we numerically calculate the specific heat $C_{2M,2N}$ defined in Eq. (8) for $\xi = 1$, and the results are shown in Figs. 17, 18, and 19, respectively, for $x = 1/2$, $x = 1$, and $y = 1$; that is, along the brown, green, and red dashed lines in Fig. 16. The specific heat $C_{2M,2N}(y)$ for the case with $x = 1/2$ and the shape factor $\xi = 1$ shown in Fig. 17(a) has two peaks at the critical points $y_{c1} = 1/2$ and $y_{c2} = 3/2$. Here the thermodynamic limit is plotted according to $C'_{\infty}(y) = 0$ for $y \leq 1/2$ and for $y \leq 3/2$, and

$$C'_{\infty}(y) = \frac{1}{4\pi} \frac{(\ln y)^2}{\sqrt{4y^2 - 1}} + \frac{9y}{4\pi} \frac{(\ln y)^2}{\sqrt{9 - 4y^2}}, \quad (47)$$

for $1/2 < y < 3/2$. The distribution of the partition function zeros for the lattice of $2M \times 2N = 32 \times 512$ is shown in Figs. 17(b) and 17(c). It is a symmetric structure, made of radial line segments. The zeros are distributed in $2M = 32$ radial line segments, and each segment has $N = 256$ zeros. The two ends of the segments on $\text{Re}(y)$ axis correspond to the two critical points. This feature is similar to that in Fig. 7(b), while the difference is that here the distribution of the zeros in the radial line segments are centered at the origin. The correlation length critical exponent ν and the shift exponent λ have been calculated numerically, and the results are $\nu = 0.854 \pm 0.001$ and $\lambda = 0.568 \pm 0.011$ for $y_{c1} = 1/2$, and $\nu = 0.843 \pm 0.003$ and $\lambda = 0.549 \pm 0.023$ for $y_{c2} = 3/2$.

The specific heat $C_{2M,2N}(y)$ for the case with $x = 1$ and the shape factor $\xi = 1$ is shown in Fig. 18(a). There is a critical point located at $y_c = 2$. The thermodynamic limit of the specific heat curve is the same as $C_{\infty}(y)$ in Eq. (40). Near $y = 0$, there are sharp but small peaks for smaller lattices, originating from the competition of the horizontal dimers with a fixed weight $x = 1$ and the vertical dimers with a varying weight y , similar to the specific heat of the K_2 -model honeycomb lattice I in Fig. 14(a). The partition function zeros of this case also have a symmetric structure, consisting of radial line segments. The zeros distribute in the radial line segments from $\text{Re}(y) \sim 0$ to $\text{Re}(y) = 2$, as shown in Fig. 18(b). Clearly

from the zoom-in of the zero distribution near the origin of the complex y plane in Fig. 18(c), the zeros do not approach the origin, thereby there is no peak at $y = 0$ in the thermodynamic limit. For this case, the correlation length critical exponent and the shift exponent are found to be $\nu = 0.848 \pm 0.002$ and $\xi = 0.563 \pm 0.011$.

The specific heat $C_{2M,2N}(x)$ and the partition function zeros for the case with $y = 1$ and $\xi = 1$ are shown in Fig. 19. The specific heat curve shown in Fig. 19(a) has a single sharp peak at $x_c = 2$, and the thermodynamic limit $C'_{\infty}(x)$ is the same as $C_{\infty}(y)$ of Eq. (40) with y replaced by x . The partition function zeros of the lattice of $2M \times 2N = 32 \times 512$ have an interesting distribution pattern with arabesque structures [see Fig. 19(b)] and the zeros do not approach the origin in the complex x plane [see Fig. 19(c)]. These structures have mirror symmetries with respect to the $\text{Re}(x)$ and $\text{Im}(x)$ axes, and are more complicated than the other two cases. Whether these structures are a deformation from simple circle and line segmental geometries require further investigations. Similar to the cases discussed above, the zeros at the end of the distribution line at $\text{Re}(x) = 2$ contribute to the peak at the critical point $x_c = 2$. Using numerical calculations, the correlation length critical exponent and the shift exponent of this case have been found to be $\nu = 0.848 \pm 0.003$ and $\xi = 0.563 \pm 0.015$.

The values of the correlation length critical exponent ν and the shift exponent λ for the above three cases are summarized in the phase diagram in Fig. 16. Despite small numerical computation errors, it is apparent that $\lambda \neq 1/\nu$.

VI. SUMMARY

We considered the dimer model on a generalized finite checkerboard B rectangular lattice that includes three different types of lattices (see Fig. 2). We have studied all these three cases. For the first case (namely, $x_1 = x_2 = x$ and $y_1 = y_2 = y$) the dimer model on the checkerboard B lattice reduces to the dimer model on the rectangular lattice [see Fig. 2(b)]. For the second case (namely, $x_1 = x_2 = x$, $y_1 = y$, $y_2 = 1$) the dimer model on the checkerboard B lattice reduces to the generalized K -model [29,30] [see Fig. 2(d)]. And finally the dimer model on the checkerboard B lattice, in the third case when one of the weights y_1 or y_2 , say y_2 is equal to zero and

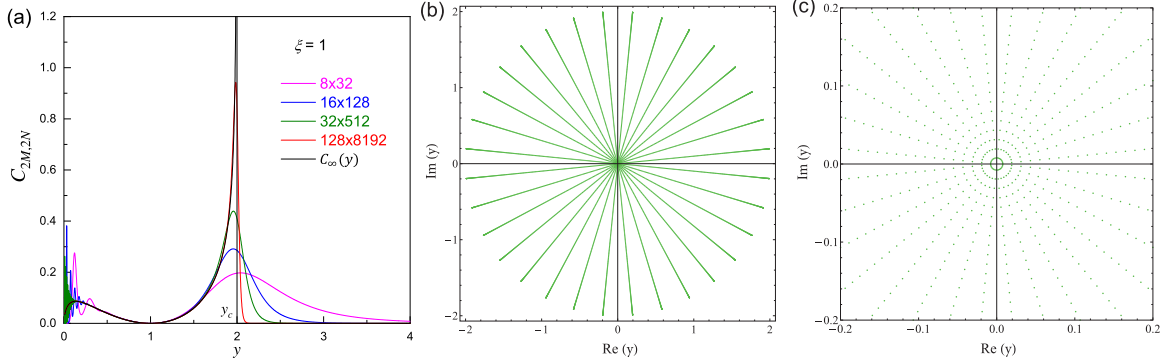


FIG. 18. The specific heat $C_{2M,2N}(y)$ of the K_2 -model honeycomb lattice II in Fig. 4(d) and $x = 1$ with the shape factor $\xi = 1$, as a function of y . Here $y_c = 2$, and $C_{\infty}(y)$ is defined in Eq. (40). (b) The partition function zeros for the lattice of $2M \times 2N = 32 \times 512$. (c) The zoom-in of (b).

the other is a free parameter, say $y_1 = y$, reduces to the dimer model on the honeycomb lattice (the K_2 -model [28]) [see Figs. 2(c) and 4(b)]. Thus, we find out that the dimer model on the checkerboard B lattice has two types of critical behaviors. In one limit this model is the anisotropic dimer model on rectangular lattice with algebraic decay of correlators and in another limit it is the anisotropic generalized Kasteleyn model with radically different critical behavior.

One type of the critical behaviors occurs when the dimer model on the checkerboard B lattice is reduced to the dimer model on the rectangular lattice. The analysis of the dimer model in that limit is quite similar to the analysis of the dimer model on the checkerboard A lattice [35]. We have considered the behavior of the specific heat near the critical point. The pseudocritical point t_{pseudo} , which is the value of the temperature at which the specific heat has its maximum for a finite $2M \times 2N$ lattice, approaches the critical point $t_c = 0$ as $L \rightarrow \infty$ in a manner dictated by the shift exponent λ ; see Eq. (2). We find that the maximum of the specific heat (at the pseudocritical point t_{pseudo}) always occurs at vanishing reduced temperature for any finite $2M \times 2N$ lattice and coincides with the critical point t_c in the thermodynamic limit ($t_{\text{pseudo}} = t_c = 0$). Hence, from Eq. (2) we found that the shift exponent is infinity, $\lambda = \infty$. This adds to the catalog of anomalous circumstances where the shift exponent is not coincident with the correlation length critical exponent.

Another type of critical behaviors occurs when the dimer model on the checkerboard B lattice is reduced to the model on the generalized K -model. To see the critical behavior of this model, we considered a particular situation with $x = 1/4$ and another situation with $y = 1$, which, respectively, correspond to varying the parameter y along the green dashed line of $x = 1/4$ and varying the parameter x along the red dashed line of $y = 1/2$ in Fig. 6. The specific heat of the former has two peaks [see Fig. 7(a)], while the latter has a single peak [see Fig. 8(a)]. From the analysis of the heights and locations of the peaks, we found that in this case the correlation length critical exponent ν and the shift exponent λ are not coincident.

In addition, we have considered in full detail the third case, namely, when the dimer model on the checkerboard B lattice reduces to the dimer model on the honeycomb lattice. The lattice anisotropy has strong effects on the behavior of the specific heat of a finite system: It has multiple peaks, whose properties are anisotropic. It transforms to a single sharp peak at the critical point accompanying with other peaks gradually smeared out as the system size becomes larger. The thermodynamic limit of the specific heat [Figs. 13(a), 14(a), 17(a), 18(a), and 19(a)] and the density of dimers [Figs. 13(a) and 14(a)] of the dimer model on the honeycomb lattice can be well described by analytical functions, and the scaling function was depicted in Fig. 15. From a finite-size analysis we have found that the lattice anisotropy dominates the values of the correlation length

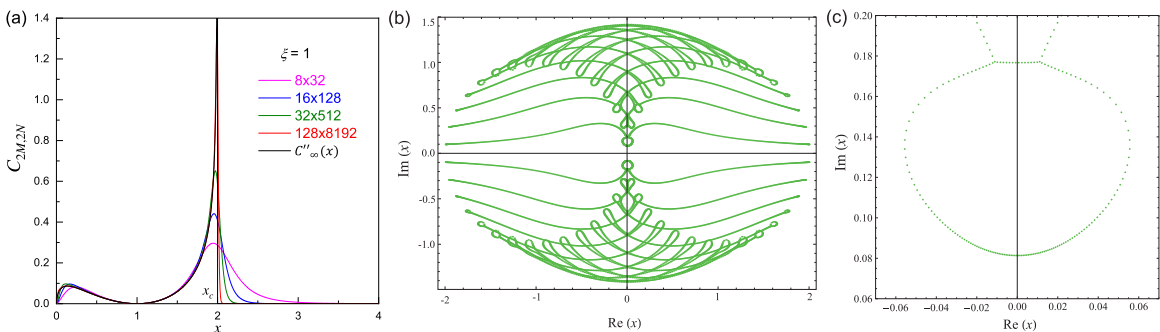


FIG. 19. The specific heat $C_{2M,2N}(x)$ of the K_2 -model honeycomb lattice II in Fig. 4(d) and $y = 1$ with the shape factor $\xi = 1$, as a function of x . Here $x_c = 2$, and $C'_{\infty}(x)$ is the same as $C_{\infty}(y)$ of Eq. (40) with y replaced by x . (b) The partition function zeros for the lattice of $2M \times 2N = 32 \times 512$. (c) The zoom-in of (b).

critical exponent ν and the shift exponent λ , and λ is generally unequal to $1/\nu$ ($\lambda \neq 1/\nu$).

Finally, to further understand the properties of the critical region, we have analyzed the partition function zeros of $2M \times 2N$ finite lattices and depicted distributions of the zeros in the complex plane. We have observed that the partition function zeros for finite-size systems can have very interesting structures, made of rings (Fig. 8), concentric circles or radial line segments (Figs. 10, 11, 17, 18), or even arabesque structures (Fig. 19). We found a general scenario that the multiple peaks in the specific heat curves can be understood from the distributions of the partition function zeros in ring, concentric circle and radial line segments, as well as in deformed patterns. A peak in the specific heat curve is a result of the ring distribution pattern of zeros, and the number of peaks is equal to the number of rings which is in principle proportional to the lattice size $2N$, or more precisely, equal to N . Meanwhile, the heights of the peaks are associated with the lattice size $2M$, due to the contributions from the specific heat components of the $2M$ zeros in a ring. This lattice anisotropy characterizes the critical behaviors of the dimer model on the checkerboard B lattice, crucially determining the values of the correlation length critical exponent ν and the shift exponent λ . It follows that the “effective” characteristic length scale for direction dependent quantities, such as ν and λ , is not necessarily equal to the system size $\sqrt{4MN}$. As there is no connection between λ and $1/\nu$ in the FSS theory, from

a theoretical perspective the discrepancy between them can be originated from the characteristic length appearing in the scaling forms of Eqs. (1) and (2). This point requires further investigation. Besides, for the case of partition function zeros distributing in radial line segments, ends of the line segments at the real axis are corresponding to the critical points in the thermodynamic limit. The transformation of the specific heat curve from the multipeak version of finite-size cases to the single-peak version in the thermodynamic limit is a result of dominant and accumulative contributions from the zeros at the two ends. This physical picture can be useful for better understanding rich and complex critical behaviors of the dimer model on the checkerboard lattices.

ACKNOWLEDGMENTS

N.S.I. thanks the Laboratory of Statistical and Computational Physics at Institute of Physics, Academia Sinica, Taipei, Taiwan, for hospitality during completion of this work. This work was partially supported by a grant from the Ministry of Science and Technology of the Republic of China (Taiwan) under Grants No. MOST 106-2112-M-001-027 and No. 107-2811-M-001-033 (C.K.H.), and MOST Grants No. 106-2112-M-008-022, No. 107-2112-M-008-012, and No. 107-2912-I-008-512 (M.C.W.), and by the RA MES State Committee of Science, in the frames of the research Project No. 18T-1C113 (N.S.I.).

-
- [1] R. H. Fowler and G. S. Rushbrooke, *Trans. Faraday Soc.* **33**, 1272 (1937).
 - [2] P. Bleher, B. Elwood, and D. Petrovic, *J. Stat. Phys.* **171**, 400 (2018).
 - [3] E. Basor and P. Bleher, *Commun. Math. Phys.* **356**, 397 (2017).
 - [4] P. A. Pearce and A. Vittorini-Orgeas, *J. Phys. A* **50**, 434001 (2017).
 - [5] E. Basor, *Random Matrices - Theory Appl.* **6**, 1740003 (2017).
 - [6] D. Alberici and P. Contucci, *Commun. Math. Phys.* **331**, 975 (2014).
 - [7] M. Disertori and A. Giuliani, *Commun. Math. Phys.* **323**, 143 (2013).
 - [8] A. Giuliani, I. Jauslin, and E. H. Lieb, *J. Stat. Phys.* **163**, 211 (2016).
 - [9] N. S. Izmailian, *Eur. Phys. J. B* **90**, 160 (2017).
 - [10] J. G. Brankov and V. B. Priezzhev, *Nucl. Phys. B* **400**, 633 (1993).
 - [11] R. Moessner and K. S. Raman, in *Introduction to Frustrated Magnetism*, edited by C. Lacroix, P. Mendels, and F. Mila (Springer, Berlin, 2011), pp. 437–479.
 - [12] L. Zdeborová and M. Mézard, *J. Stat. Mech.* (2006) P05003.
 - [13] A. Barra, P. Contucci, R. Sandell, and C. Vernia, *Sci. Rep.* **4**, 4174 (2014).
 - [14] D. S. Rokhsar and S. A. Kivelson, *Phys. Rev. Lett.* **61**, 2376 (1988).
 - [15] S. Franco, A. Hanany, D. Vegh, B. Wecht, and K. D. Kennaway, *J. High Energy Phys.* **01** (2006) 096.
 - [16] N. S. Izmailian, C.-K. Hu, and R. Kenna, *Phys. Rev. E* **91**, 062139 (2015).
 - [17] M. E. Fisher and J. Stephenson, *Phys. Rev.* **132**, 1411 (1963).
 - [18] R. E. Hartwig, *J. Math. Phys. (New York)* **7**, 286 (1966).
 - [19] N. S. Izmailian, V. B. Priezzhev, P. Ruelle, and C.-K. Hu, *Phys. Rev. Lett.* **95**, 260602 (2005).
 - [20] N. S. Izmailian, V. B. Priezzhev, and P. Ruelle, *SIGMA* **3**, 001 (2007).
 - [21] A. Morin-Duchesne, J. Rasmussen, and P. Ruelle, *J. Phys. A* **49**, 174002 (2016).
 - [22] N. S. Izmailian, R. Kenna, W. Guo, and X. Wu, *Nucl. Phys. B* **884**, 157 (2014).
 - [23] P. A. Pearce and J. Rasmussen, *J. Stat. Mech.* (2007) P02015.
 - [24] P. Ruelle, *J. Phys. A* **46**, 494014 (2013).
 - [25] P. Ruelle, *J. Stat. Mech.* (2007) P09013.
 - [26] N. Allegra, *Nucl. Phys. B* **894**, 685 (2015).
 - [27] R. Kenyon, *Ann. Probab.* **29**, 1128 (2001).
 - [28] C. S. O. Yokoi, J. F. Nagle, and S. R. Salinas, *J. Stat. Phys.* **44**, 729 (1986).
 - [29] J. F. Nagle, *J. Chem. Phys.* **58**, 252 (1973).
 - [30] S. M. Bhattacharjee and J. F. Nagle, *Phys. Rev. A* **31**, 3199 (1985).
 - [31] P. W. Kasteleyn, *J. Math. Phys.* **4**, 287 (1963).
 - [32] F. Y. Wu, *Phys. Rev.* **168**, 539 (1968).
 - [33] J. C. Slater, *J. Chem. Phys.* **9**, 16 (1941).
 - [34] H. Takahashi, *Proc. Phys. Math. Soc. (Japan)* **23**, 1069 (1941).
 - [35] N. S. Izmailian, M.-C. Wu, and C.-K. Hu, *Phys. Rev. E* **94**, 052141 (2016).
 - [36] H. Cohn, R. Kenyon, and J. Propp, *J. Am. Math. Soc.* **14**, 297 (2001).

- [37] M. Fisher and M. N. Barber, *Phys. Rev. Lett.* **28**, 1516 (1972).
- [38] *Finite-size Scaling and Numerical Simulation of Statistical Systems*, edited by V. Privman (World Scientific, Singapore, 1990).
- [39] C.-K. Hu, *Chinese J. Phys.* **52**, P1 (2014).
- [40] S. Kawata, H.-B. Sun, T. Tanaka, and K. Takeda, *Nature* **412**, 697 (2001).
- [41] V. F. Puntas, K. M. Krishnan, and A. P. Alivisatos, *Science* **291**, 2115 (2001).
- [42] Y. Yin, R. M. Rioux, C. K. Erdonmez, S. Hughes, G. A. Somorjai, and A. P. Alivisatos, *Science* **304**, 711 (2004).
- [43] A. E. Ferdinand, *J. Math. Phys.* **8**, 2332 (1967).
- [44] E. Ivashkevich, N. S. Izmailian, and C.-K. Hu, *J. Phys. A* **35**, 5543 (2002).
- [45] B. Nienhuis, H. J. Hilhorst, and H. Blöte, *J. Phys. A* **17**, 3559 (1984).
- [46] C. Itzykson, H. Saleur, and J. B. Zuber, *Europhys. Lett.* **2**, 91 (1986).
- [47] F. Y. Wu, W.-J. Tzeng, and N. S. Izmailian, *Phys. Rev. E* **83**, 011106 (2011).
- [48] N. S. Izmailian, K. B. Oganesyan, M.-C. Wu, and C.-K. Hu, *Phys. Rev. E* **73**, 016128 (2006).
- [49] N. S. Izmailian and R. Kenna, *Phys. Rev. E* **84**, 021107 (2011).
- [50] N. S. Izmailian, K. B. Oganesyan, and C.-K. Hu, *Phys. Rev. E* **67**, 066114 (2003).
- [51] C. Nash and D. O'Connor, *J. Phys. A* **50**, 355002 (2017).
- [52] Y. Kong, *Phys. Rev. E* **74**, 011102 (2006).
- [53] Y. Kong, *Phys. Rev. E* **74**, 061102 (2006).
- [54] G. Pogudin, *Phys. Rev. E* **96**, 033303 (2017).
- [55] X. Wu and N. Izmailyan, *Phys. Rev. E* **91**, 012102 (2015).
- [56] X. Wu, R. Zheng, N. S. Izmailian, and W. Guo, *J. Stat. Phys.* **155**, 106 (2014).
- [57] X. Wu, N. S. Izmailian, and W. Guo, *Phys. Rev. E* **87**, 022124 (2013).
- [58] X. Wu, N. S. Izmailian, and W. Guo, *Phys. Rev. E* **86**, 041149 (2012).
- [59] J. L. Cardy, *Finite-Size Scaling* (North Holland, Amsterdam, 1988).
- [60] M. N. Barber, in *Phase Transition and Critical Phenomena*, edited by C. Domb and J. L. Lebowitz (Academic Press, New York, 1983), Vol. 8.
- [61] A. E. Ferdinand and M. E. Fisher, *Phys. Rev.* **185**, 832 (1969).
- [62] O. Diego, J. González, and J. Salas, *J. Phys. A* **27**, 2965 (1994).
- [63] S. Y. Kim, *J. Korean Phys. Soc.* **72**, 646 (2018).
- [64] W. Janke and R. Kenna, *Phys. Rev. B* **65**, 064110 (2002).
- [65] C.-N. Chen, Y.-H. Hsieh, and C.-K. Hu, *Europhys. Lett.* **104**, 20005 (2013); Y.-H. Hsieh, C.-N. Chen, and C.-K. Hu, *EPJ Web Conf.* **108**, 01005 (2016).
- [66] Y.-H. Hsieh, C.-N. Chen, and C.-K. Hu, *Comput. Phys. Commun.* **209**, 27 (2016).
- [67] S. Y. Kim, R. J. Creswick, C.-N. Chen, and C.-K. Hu, *Physica A (Amsterdam)* **281**, 262 (2000).
- [68] C.-N. Chen, C.-K. Hu, and F. Y. Wu, *Phys. Rev. Lett.* **76**, 169 (1996); F. Y. Wu, G. Rollet, H. Y. Huang, J. M. Maillard, C.-K. Hu, and C.-N. Chen, *ibid.* **76**, 173 (1996).
- [69] K. Ishida, M. Morishita, K. Yawata, and H. Fukuyama, *Phys. Rev. Lett.* **79**, 3451 (1997).
- [70] R. G. Melko, B. C. den Hertog, and M. J. P. Gingras, *Phys. Rev. Lett.* **87**, 067203 (2001).
- [71] S. Lucas, K. Grube, C.-H. Huang, A. Sakai, W. Wunderlich, E. L. Green, J. Wosnitzer, V. Fritsch, P. Gegenwart, O. Stockert, and H. V. Löhneysen, *Phys. Rev. Lett.* **118**, 107204 (2017).
- [72] H. A. Zad and N. Ananikian, *J. Phys.: Condens. Matter* **30**, 165403 (2018).
- [73] A. P. Ramirez, A. Hayashi, R. J. Cava, R. Siddharthan, and B. S. Shastry, *Nature (London)* **399**, 333 (1999).
- [74] E. Jurčičinová and M. Jurčičin, *Phys. Rev. E* **97**, 052129 (2018).
- [75] J. F. Nagle, *Phys. Rev. Lett.* **34**, 1150 (1975).
- [76] J. Villain, in *Ordering in Strongly Fluctuating Condensed Matter Systems*, edited by T. Riste (Plenum, New York, 1980).
- [77] S. M. Bhattacharjee, J. F. Nagle, D. A. Huse, and M. E. Fisher, *J. Stat. Phys.* **32**, 361 (1983).
- [78] M.-C. Wu, C.-K. Hu, and N. S. Izmailian, *Phys. Rev. E* **67**, 065103(R) (2003).